# Systematics of $^8$Li-induced radioactive beam reactions: $E$=13–20 MeV

F. D. Becchetti, W. Z. Liu,* K. Ashktorab,† J. F. Bajema, J. A. Brown, J. W. Jänecke, and D. A. Roberts
*Physics Department, University of Michigan, Ann Arbor, Michigan 48109-1090*

J. J. Kolata, K. L. Lamkin, A. Morsad,‡ R. J. Smith,§ and X. J. Kong**
*Physics Department, University of Notre Dame, Notre Dame, Indiana 46556*

R. E. Warner
*Physics Department, Oberlin College, Oberlin, Ohio 44074*
(Received 21 December 1992)

Elastic and inelastic scattering, one-nucleon transfers [mostly ($^8$Li,$^7$Li)] and the ($^8$Li,$\alpha$) fusion-evaporation reaction have been studied on a variety of targets ($A$=1–58) at $E(^8\text{Li}) \approx$ 13–20 MeV using the University of Michigan–University of Notre Dame radioactive nuclear beam (RNB) facility. The latter, which produces an energy-resolved ($\sim$ 500 keV FWHM), focused beam with intensity $\gtrsim 10^6$ $^8$Li/s, permitted measurements to selected nuclear levels with cross sections down to approximately 1 mb/sr. Based on the systematics of the measured $^8$Li elastic scattering an appropriate $^8$Li optical potential was deduced. Large inelastic scattering cross sections (and $B[E2\uparrow]$) are observed for $^8\text{Li}\rightarrow{}^8\text{Li}^*_{0.98}$. Large cross sections are also observed for the ($^8$Li,$^7$Li) transfer reaction corresponding to quasielastic (viz., $Q \approx 0$) neutron transfer to selected high spin excited levels in the residual nucleus. The ($^8$Li, $\alpha$) fusion-evaporation reaction also appears to be significant and can produce very-high-energy $\alpha$ particles, viz., $E_\alpha \gg E_{\text{beam}}$. Although observed using $^8$Li, these features appear to be important for many RNB-induced reactions and they must be considered, for example, in nucleosynthesis calculations involving $^8$Li and other short-lived radioactive nuclei.

PACS number(s): 25.70.Bc, 25.70.De, 25.70.Gh, 25.70.Hi

## I. INTRODUCTION

Reactions involving short-lived radioactive nuclear beams (RNB) are of intrinsic interest in nuclear physics and nuclear astrophysics because they can involve unusual isospin, spin, and energy transfer [1–4]. In contrast to similar reactions involving beta-stable nuclei, reactions involving $^8$Li (and other RNB) generally can have reaction $Q$ values for certain transitions which are close to the optimum ($Q_{\text{opt}}$) for maximum cross section [5,6]. Furthermore, the existence [7] of a neutron (or proton) "halo" or "skin" in a RNB projectile may result in enhanced transfer reaction modes [5] and unique inelastic projectile excitations such as a soft-$E1$ dipole excitation [8,9].

There is obviously considerable interest in the study of RNB-induced reactions for nucleosynthesis calculations. As a well-known example, the measured abundances of the lithium isotopes provide constraints on the initial baryon density deduced for the early Universe [1–3]. One cannot both reproduce these abundances and, using standard nucleosynthesis models [1], have a large enough baryon density ($\Omega = 1$) to close the universe. Inhomogeneous big-bang models (IBB), and other nonstandard nucleosynthesis models, are thus being invoked [2–4]. The IBB model uses nonuniform initial baryon densities and postulates unusual nuclear reaction chains, such as those involving $^8$Li and other short-lived radioactive nuclei, to produce many of the heavy elements. However, reactions with $Q \gg 0$, which are typical of $^8$Li-induced and other RNB reactions, may have large reaction cross sections. This may occur even at low collisional energies due to nucleon tunneling, fusion evaporation, and other mechanisms allowed by the large energies released. It is therefore difficult to decide *a priori* which radioactive nuclei and which specific reactions will be important at low, astrophysically relevant, center-of-mass energies. Assumptions made concerning reaction rates of radioactive nuclei in nucleosynthesis calculations may therefore be incomplete or even erroneous. The experimental study of RNB reaction mechanisms and the most important RNB reaction channels is therefore important.

*Present address: Texas A&M University, Cyclotron Institute, College Station, TX 77843.
†Present address: Physics Division, Brookhaven National Laboratories, Upton, NY 11973.
‡Permanent address: Centre Nationale de Recherches, Scientifique, Groupe PNIN, 23 rue du Loess, 67000 Strasbourg, France.
§Present address: Division of Nuclear Medicine, Department of Radiology, Hospital of The University of Pennsylvania, Philadelphia, PA 19104.
**Present address: Shanghai Institute of Nuclear Physics, People's Republic of China.

 

Low-energy, energy-resolved radioactive nuclear beams (RNB) with intensities sufficient to observe some of the most significant RNB reaction channels have recently been developed by us and others [10–12]. As part of these measurements, we have made a systematic study of $^8$Li (and other) RNB-induced reactions at low bombarding energies ($E_{\rm lab} < 20$ MeV) involving a variety of light and heavy targets. Some initial sets of measurements have previously been reported [5,6,10–17], along with selected studies on individual target nuclei [16–20]. Here we present systematics for a range of targets.

## II. EXPERIMENTAL SETUP

The experiments used $^8$Li beams produced using the University of Michigan 3.5 T superconducting solenoid installed at the University of Notre Dame FN tandem Van de Graaff accelerator [10–12]. A negative Cs-ion sputter source produces 1 to 10 electrical $\mu$A of primary $^7$Li beam, resulting in secondary $^8$Li beams of $10^5$ to $10^7$/s at $E(^8\text{Li}) \doteq 14.3$–14.9 MeV and 19.3–19.9 MeV, with 350 to 600 keV FWHM energy spread. This beam was focused to a spot approximately 5 mm in diameter, with a $\pm 3°$ angular spread on the secondary target. The secondary beam purity was typically 70–80 % $^8$Li, depending on the solenoid collimation, with the major impurities being $^4\text{He}^{2+}$ [5–10 %; $E \approx \frac{8}{9}E(^8\text{Li})$], $^6\text{He}^{2+}$[2–5 %; $E \approx \frac{16}{27}E(^8\text{Li})$], $^7\text{Li}^{2+}$[2–5 %; $E \approx \frac{1}{2}E(^8\text{Li})$] as well as lesser amounts of $^2\text{H}^{1+}$, $^4\text{He}^{1+}$, $^8\text{Li}^{2+}$, $^{12}\text{B}^{4,5+}$, and other low-energy ions. Thus, owing to its high magnetic rigidity, $^8\text{Li}^{3+}$ was the highest-energy component in the focused RNB and hence reactions with $Q > 0$ were usually identified unambiguously.

Secondary, scattered reaction products were identified using a $\Delta E$-$E$-$XY$ counter telescope with a silicon surface-barrier (SiSB) $\Delta E$ detector (10 to 28 $\mu$m thick) backed by a 25 × 25 mm$^2$ position-sensitive SiSB $E$ detector (PSD) ~ 200 $\mu$m thick. The primary and secondary beam intensities were monitored with additional SiSB detectors. The RNB apparatus (superconducting solenoid) and detection system ($\Delta E$-$E$-$XY$ Si telescope) are described in more detail in Refs. [10–12]. The prominent reactions studied, their $Q$ values, and the corresponding targets used in the present experiments (compositions and thicknesses) are listed in Table I.

## III. ELASTIC AND INELASTIC SCATTERING

### A. Elastic data

Targets $^{\rm nat,13}\text{CH}_2$, $^{\rm nat}\text{CD}_2$, $^9$Be, $^{12,13}$C, Melamine ($^{\rm nat}\text{C}_3$ $^{\rm nat}\text{H}_6$ $^{14}\text{N}_6$), $^{27}$Al, $^{\rm nat}$Ti, $^{\rm nat}$Ti $\text{D}_2$, $^{\rm nat}$Ni, and $^{\rm nat}$Au of thickness 0.4 to 3 mg/cm$^2$ have been used for study of elastic scattering. The gold target was used primarily for normalization to Rutherford scattering. Selected particle identification spectra ($\Delta E$-$E$) are given in Figs. 1–3. Gated and projected $^8$Li elastic and inelastic energy spectra and ($^8$Li,$^7$Li) reaction spectra are shown in Figs. 4–6. In some cases, the energy spectra have been corrected for kinematic shifts, i.e., $dE/d\theta$, using the $XY$ information available from the SiSB PSD.

The $^8$Li elastic angular distributions are shown in Figs. 7 and 8. The accuracy of the forward-angle elastic scattering data is limited by the $\pm 3°$ spread in the secondary RNB combined with the rapid falloff ($\sim 1/\theta^4$) of the elastic scattering versus $\theta$. In certain cases ($\theta_{\rm lab} < 20°$) it was necessary to determine a scattering angle weighted by an assumed Rutherford scattering cross section. At larger angles, the data are shown with the angular divergence indicated as an uncertainty in the scattering angle. The overall uncertainties in the normalizations are estimated to be ±20% due mostly to uncertainties in relative target thicknesses and the secondary RNB integration.

### B. Optical-model analysis and strong absorption radii

Analyses of the elastic and inelastic scattering data for $^8$Li + $^{12}$C and $^8$Li + $^{58}$Ni at $E \doteq 14$ MeV are presented in Refs. [16] and [17], respectively. The $^8$Li+$^{12}$C optical model (OM) parameter set deduced [16] at $E = 14$ MeV was used as a basis for analysis of the $^8$Li elastic data

TABLE I. Transfer reactions and targets studied.

| Reaction | g.s.→g.s. $Q$ value (MeV) | Target composition | Thickness (mg/cm$^2$) |
|---|---|---|---|
| $^2$H($^8$Li,$^7$Li)$^3$H | 4.224 | $^{\rm nat}\text{TiD}_2$ | 2.72 ± 0.03 |
| | | $^{\rm nat}\text{CD}_2$ | 1.9 ± 0.1 |
| $^9$Be($^8$Li,$^7$Li)$^{10}$Be | 4.779 | $^9$Be | 1.8 ± 0.1 |
| $^9$Be($^8$Li, $\alpha$)$^{13}$B | 13.308 | " | " |
| $^{12}$C($^8$Li,$^7$Li)$^{13}$C | 2.913 | $^{\rm nat}$C | 2.2 ± 0.1 |
| $^{12}$C($^8$Li, $\alpha$)$^{16}$N | 12.84 | $^{\rm nat}$C | 1.0 ± 0.1 |
| | | $^{\rm nat}$C | 0.59 ± 0.06 |
| $^{13}$C($^8$Li,$^7$Li)$^{14}$C | 6.143 | $^{13}\text{CH}_2$ | 0.54 ± 0.02 |
| | | $^{13}$C | 1.0 ± 0.1 |
| $^{14}$N($^8$Li,$^7$Li)$^{15}$N | 8.801 | $\text{C}_3\text{N}_6\text{H}_6$ | 0.9 ± 0.1 |
| $^{27}$Al($^8$Li,$^7$Li)$^{28}$Al | 5.693 | $^{\rm nat}$Al | 1.3 ± 0.1 |
| $^{58}$Ni($^8$Li,$^7$Li)$^{59}$Ni | 6.967 | $^{\rm nat}$Ni | 1.1 ± 0.1 |

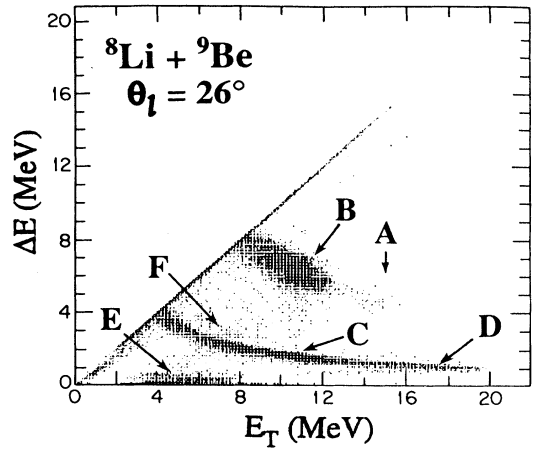


FIG. 1. $^8$Li + $^9$Be $\Delta E$-$E$ spectrum, $E(^8\text{Li}) \doteq 14$ MeV, taken with a $\sim 2$ mg/cm$^2$ Be target. Group "A" is identified as $^9\text{Be}(^8\text{Li},^7\text{Li})\ ^{10}\text{Be}_{\text{g.s.}}$ (see also Fig. 2).

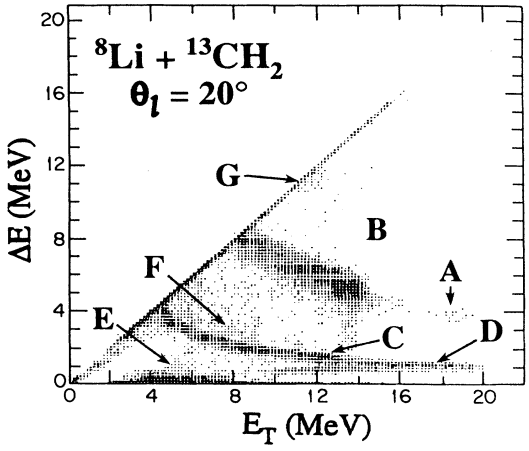


FIG. 3. $^8$Li + $^{13}$C $\Delta E$-$E$ spectrum at $E(\text{Li}) = 14$ MeV from a 1 mg/cm$^2$ enriched $^{13}CH_2$ foil. Group "A" is identified as $^{13}\text{C}(^8\text{Li},^7\text{Li})^{14}\text{C}_{\text{g.s.}}$ (see also Fig. 2).

from other targets. Since our experimental setup was not optimized for measurements of elastic scattering, we have somewhat limited angular distributions for targets other than $^{12}$C. In addition, rather wide $\Delta E$-$E$-$XY$ detector angular acceptances ($\Delta\theta$) of $\pm 3°$ to $\pm 6°$ were used. Nonetheless, it is possible to extract several meaningful features of the low-energy $^8$Li RNB optical-model potentials from fits to the elastic data.

Starting with the fitted $^8$Li + $^{12}$C OM parameters, and using published [18–21] analyses of $^{6,7}$Li elastic scattering on light targets as a guide, we adjusted [22] individual OM parameters (such as potential strengths or radii) as

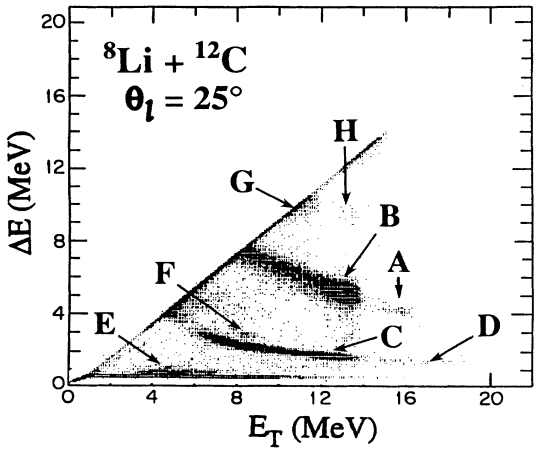


FIG. 2. $^8$Li + $^{12}$C $\Delta E$-$E$ spectrum, $E(^8\text{Li}) \doteq 14$ MeV, from an 0.59 mg/cm$^2$ natural carbon target. Group "A" is identified as $^{12}\text{C}(^8\text{Li},^7\text{Li})^{13}\text{C}_{\text{g.s.}}$; group "B" is $^8\text{Li}^{3+}$ from $^8$Li + $^{12}$C; group "C" is $^4\text{He}^{2+}$ from $^4$He+$^{12}$C due to a $^4$He beam impurity; group "D" is high-energy $\alpha$ particles from $^{12}\text{C}(^8\text{Li}, \alpha)$; groups "E","F", and "G" arise from $^2\text{H}^{1+}$, $^6\text{He}^{2+}$, and $^9\text{Be}^{5+}$ beam impurities while group "H" is tentatively identified as $^9$Be from $^{12}\text{C}(^8\text{Li},^9\text{Be})^{11}\text{B}$.

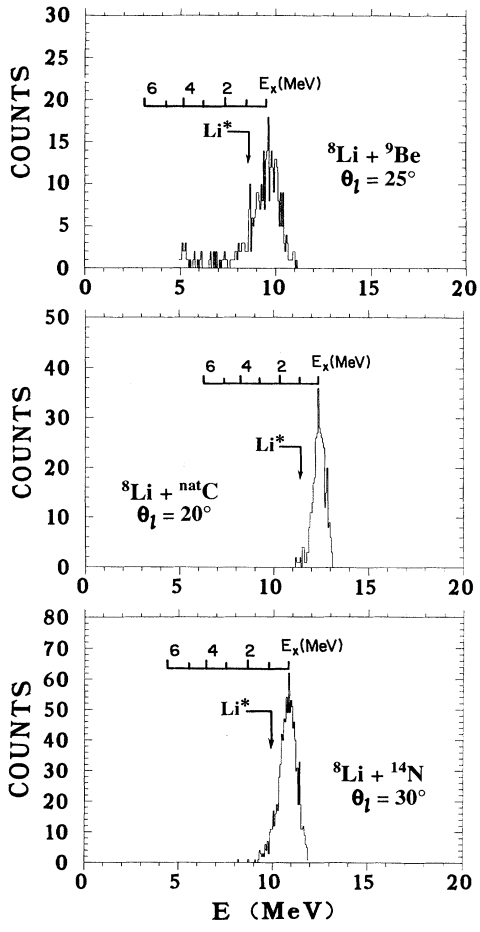


FIG. 4. Energy spectra from $^8$Li scattering on various targets, $E(^8\text{Li}) \doteq 14$ MeV.

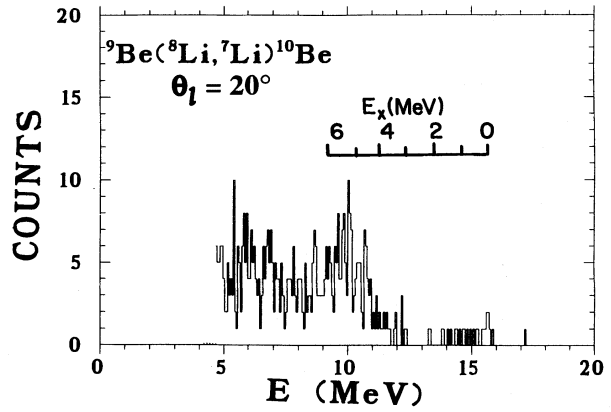


FIG. 5. Gated and projected $^9$Be($^8$Li,$^7$Li)$^{10}$Be spectrum, $E(^8\text{Li}) \doteq 14$ MeV.

a function of target mass ($A_T$), keeping the remaining parameters fixed. The exception to this was the absolute normalization, which was adjusted within its uncertainty, typically ±20%. We found, in analogy with the $^6$Li global fits given in Ref. [20], that most of the $^8$Li data could be adequately fitted (Fig. 7) by varying only the imaginary volume absorptive strength, $W$ (Table II). The latter, at least for $E(^8\text{Li}) = 13$ to 19.6 MeV, is given approximately by

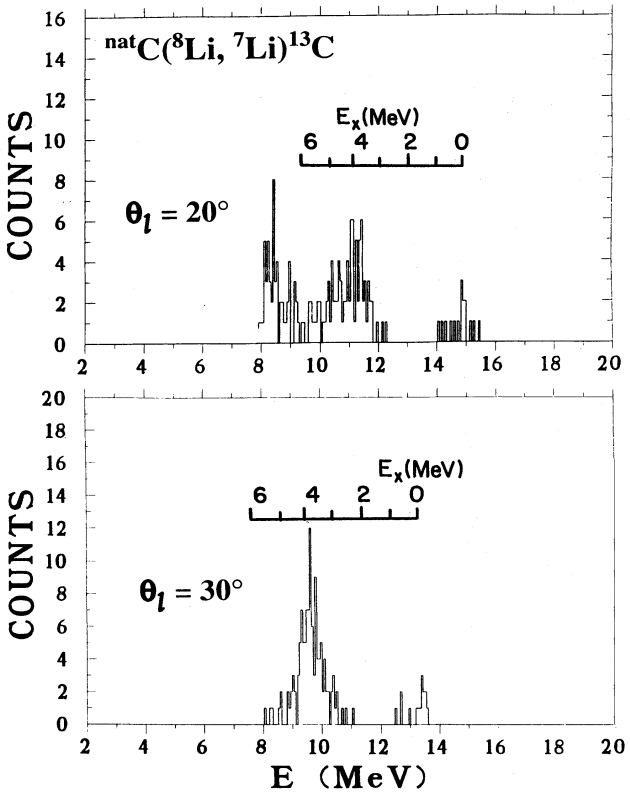


FIG. 6. Gated and projected $^{nat}$C($^8$Li,$^7$Li)$^{13}$C spectra, $E(^8\text{Li}) \doteq 14$ MeV.

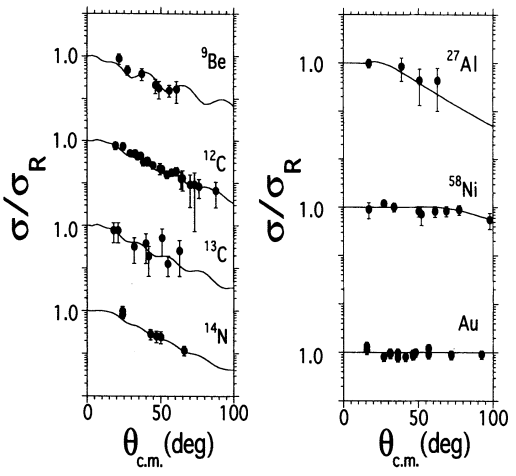


FIG. 7. Elastic scattering angular distributions for $^8$Li, $E(^8\text{Li}) \doteq 14$ MeV, compared with optical model calculations. See Table II.

$$W = 19 - 0.3A_T \text{ MeV} \quad (1)$$

where $A_T$ is the target mass. Our radius convention for $R_R$ and $R_I$ conforms to that of the folding model [20,21] where $R \approx r_0 A_T^{\frac{1}{3}}$. The projectile size is thus included in the diffuseness parameters $a_R$ and $a_I$ (Table II) which

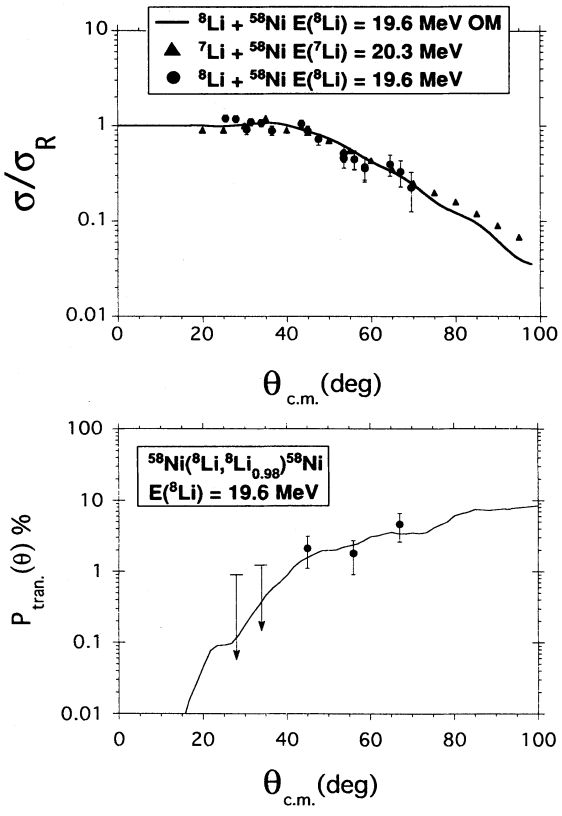


FIG. 8. Elastic and inelastic measured and calculated angular distributions for $^8$Li + $^{nat}$Ni compared with $^7$Li data [23].

TABLE II. Optical-model parameters, $E(^8\text{Li})\doteq 14$ MeV.

| System | $V_R$[a] (MeV) | $R_R$ (fm) | $a_R$ (fm) | $W$[b] (MeV) | $R_I$ (fm) | $a_I$ (fm) | $\sigma_R$[c] (mb) |
|---|---|---|---|---|---|---|---|
| $^8$Li + $^9$Be | 175 | 2.70 | 0.8 | 18.4 | 4.68 | 0.8 | 1423 |
| $^8$Li + $^{12}$C | 175 | 2.97 | 0.8 | 15.1 | 5.15 | 0.8 | 1363 |
| $^8$Li + $^{13}$C | 175 | 3.06 | 0.8 | 15.0 | 5.29 | 0.8 | 1432 |
| $^8$Li + $^{14}$N | 175 | 3.13 | 0.8 | 14.9 | 5.42 | 0.8 | 1375 |
| $^8$Li + $^{27}$Al | 175 | 3.89 | 0.8 | 11.4 | 6.75 | 0.8 | 1302 |
| $^8$Li + $^{58}$Ni | 175 | 5.03 | 0.8 | 4.0 | 8.7 | 0.8 | 501[d] |

[a]Volume Woods-Saxon potential; $R_R = r_{OR}\,A_T^{\frac{1}{3}}$, $r_{OR} = 1.30$; $R_C = 1.3 \times (A_T^{\frac{1}{3}} + 8^{\frac{1}{3}})$.

[b]Volume Woods-Saxon potential; $R_I = r_{OI}\,A_T^{\frac{1}{3}}$, $r_{OI} = 2.25$.

[c]Calculated reaction cross section.

[d] $^8$Li + Ni at $E(^8\text{Li})\doteq$ 14 MeV is near the Coulomb barrier (see text).

increases the mean-square optical-model radii relative to those of the corresponding nucleon-nucleus scattering potentials.

It is interesting to note that our $^8$Li parameters also give a reasonable fit to published [18,19] data for $^7$Li + $^{12}$C elastic scattering at $E \lesssim 40$ MeV. Therefore, we have adopted the $^8$Li OM parameters for both the incoming ($^8$Li) and outgoing ($^7$Li) channels in our ($^8$Li,$^7$Li) reaction calculations (see below). Although our $^8$Li potentials appear to reproduce the elastic scattering and other data quite well, they do not necessarily correspond to the potentials one would extrapolate from the "unique" $^6$Li OM potentials determined from analysis of high-energy large-angle rainbow scattering [21], as the latter potentials predict quite different volume integrals for the real and imaginary $^8$Li OM potentials than do our "best fit" sets.

Since the $^8$Li projectile has $J^\pi_{\text{g.s.}} = 2^+$, one might expect spin-orbit ($\boldsymbol{\ell}\cdot\mathbf{s}$) or similar spin-spin ($\mathbf{s}\cdot\mathbf{s}$) interactions to be enhanced in the $^8$Li OM. However, as observed [20,21,23] with $^6$Li (where $J^\pi_{\text{g.s.}} = 1^+$), such effects appear to be rather small and would probably be significant, if at all, only at much higher bombarding energies. Thus we did not include an explicit spin-orbit interaction in our $^8$Li OM.

A comparison of $^{6,7}$Li + $^{58}$Ni [23] with $^8$Li + $^{\text{nat}}$Ni scattering at $E(\text{Li}) \doteq 20$ MeV is shown in Fig. 8. As seen with $^8$Li + $^{12}$C data [16], the $^8$Li elastic scattering resembles that measured for $^{6,7}$Li, i.e., there are no anomalous effects apparent in the $^8$Li data, nor the resulting $^8$Li optical-model parameters (see below).

For the adopted $^8$Li OM potentials we have calculated the reaction cross sections ($\sigma_A$). As observed by Tanihata *et al.* [7], $^8$Li does not exhibit the anomalously large absorption cross sections noted in the most neutron-rich RNB's, such as $^{11}$Li.

### C. Inelastic scattering and $B[E2\uparrow]$ for $^8\text{Li}^*_{0.98}$

Besides elastic scattering, only weak inelastic transitions to the target levels $^{12}$C* ($2^+, E_x = 4.4$ MeV) and $^{14}$N*($0^+, E_x = 2.3$ MeV) were observed. Relatively strong projectile excitation of $^8$Li* ($2^+, E_x = 0.98$ MeV) was also observed particularly for the $^{12}$C and $^{\text{nat}}$Ni targets. The latter is attributed to nuclear and Coulomb excitation, and the analysis of the data obtained at E($^8$Li) $\doteq$ 14 MeV has been presented in detail elsewhere [16,17]. These measurements of $^8\text{Li}^*_{0.98}$ indicate a $B[E2\uparrow]$ of 25 to 70 $e^2\,\text{fm}^4$ i.e., $\gtrsim$ 30 single-particle units. This is substantially larger than $B[E2\uparrow]$ observed for $^7$Li (8 single-particle units) but is similar to that known for other very proton- and neutron-rich nuclei such as $^{10}$C and $^{10}$Be.

Additional inelastic scattering data for $^8\text{Li}^*_{0.98}$ [from $^{\text{nat}}$Ni at $E(^8\text{Li}) = 19.6$ MeV] are shown in Fig. 8, together with a distorted-wave Born-approximation (DWBA) calculation [24]. The latter includes both Coulomb and nuclear excitation with the conventional, destructive interference between them. This interference can result in a slight dip in the inelastic cross section near the grazing angle, which for our data is near $\theta_{\text{lab}} \doteq 70°$ and hence just beyond the last data point. Such an interference phenomenon could eventually be exploited to deduce detailed information about deformation parameters of the neutron and proton distributions which would be of special interest for very neutron-rich and proton-rich RNB's. Here, although limited, the data appear compatible with our measurements at $E(^8\text{Li}) \doteq 14$ MeV, viz., $B[E2\uparrow]$ of 30 to 50 $e^2\,\text{fm}^4$ for $^8\text{Li}^*_{0.98}$. However, a slight difference ($\leq$30%) in the Coulomb and nuclear $B[E2\uparrow]$ values cannot be excluded. Such differences might be expected in a nucleus such as $^8$Li where $N \gg Z$. Data at higher bombarding energies may exhibit these differences more strongly and thus should be pursued as the appropriate RNB's become available.

We have also used the measured $^8$Li* inelastic data, 1 MeV $< E_x <$ 2 MeV, to set a limit [16,17] on any low-lying soft-$E1$ dipole excitation of $^8$Li. However, we note that $^8$Li is unstable to decay to $^7\text{Li} + n$ above $E_x(^8\text{Li}) \approx$ 2 MeV, so projectile excitation above 2 MeV would not be seen in the $^8$Li spectra.

## IV. TRANSFER REACTIONS

### A. Data

Projected $\Delta E$-$E$ ($^8$Li,$^7$Li) spectra for 14 MeV $^8$Li ions on $^9$Be and $^{12}$C are shown in Figs. 5 and 6. (Related

data for $^{nat}$Ni + $^8$Li at $E \doteq 19.6$ MeV will be presented [25] elsewhere.) The identification of the ($^8$Li,$^7$Li) neutron transfer groups was rather unambiguous since, e.g., $Q \doteq +6$ MeV for $^{13}$C($^8$Li,$^7$Li)$^{14}$C and thus (Fig. 2) the $^7$Li transfer products are well separated from the $^8$Li elastic and beam-impurity scattering groups. In addition to high-energy $^7$Li, one also notes the presence of very-high-energy $\alpha$ particles with $E_\alpha$ approaching 30 MeV, i.e., at energies much greater than the beam energy. These $\alpha$ particles could be produced via ($^8$Li, $\alpha$). This, as we will discuss, is compatible with nondirect mechanisms such as compound nucleus fusion evaporation and, perhaps, sequential $^8$Li breakup. Some additional evidence for the latter was seen in the $\Delta E - E$ spectra of $^8$Li + $^{1,2}$H [6,11]. These exhibit several bands attributable to the unresolved detection of coincident light-ion fragments in the large solid angle (300 mm$^2$, 20 msr) $\Delta E$-$E$ SiSB telescope. The ($^8$Li, $\alpha$) data will be discussed in more detail in Sec. V.

In the $\Delta E$-$E$ SiSB spectra (and others presented elsewhere [5–19]) the most dominant $^8$Li-induced transfer reaction appears to be the highly exothermic single-neutron transfer reaction ($^8$Li,$^7$Li). Similarly, the reaction ($^7$Li,$^6$Li) has been shown to be a dominant channel in $^7$Li-induced reactions [19]. As previously noted, the low binding energy of the last neutron in $^8$Li (hence $Q > 0$) and the large spectroscopic [26] overlap $^8$Li$_{g.s.} \rightarrow ^7$Li$_{g.s.} + n$ (Table III) can result in large ($^8$Li,$^7$Li) cross sections even at relatively low $^8$Li bombarding energies. Likewise, the exothermic reaction ($^8$Li,$^9$Be) was observed, but with lower cross sections, and for only a few very light targets such as $^2$H. These lower cross sections result from the higher Coulomb barrier for the $^9$Be ejectile which suppresses the cross section at $E$(Li) $\leq$ 14 MeV. In contrast to the ($^8$Li,$^7$Li) and ($^8$Li,$^9$Be) reactions, ($^8$Li,$^9$Li) typically has a large negative $Q$ value and does not appear to have significant cross section, at least at $E(^8\text{Li}) \doteq 14$ MeV.

Some gated and projected ($^8$Li,$^7$Li) energy spectra are displayed in Figs. 5 and 6. Although we do not always completely resolve the $^7$Li$_{g.s.}$ from $^7$Li* ($E_x = 0.47$ MeV), particularly for measurements using targets with thicknesses $> 1$ mg/cm$^2$ (Table I), it appears that ($^8$Li,$^7$Li$_{g.s.}$) is the dominant neutron transfer mode as the groups observed were not double peaked [5], at least within the limited statistics obtained. In several targets, excited target levels at $E_x > 3$ MeV were also observed. Due to their incomplete separation from the much more intense elastically and inelastically scattered $^8$Li ions, we could not always extract clean ($^8$Li,$^7$Li) spectra. However, separate measurements made for $^8$Li+$^{12}$C allowed for cleaner separation of $^7$Li from $^8$Li and provided $^{12}$C($^8$Li,$^7$Li) reaction spectra which extended to high excitation in $^{13}$C.

Absolute transfer-reaction cross sections were obtained from $^8$Li beam normalizations deduced from direct $\theta = 0°$ RNB flux measurements using a reduced secondary beam, or from Rutherford scattering of $^8$Li from a gold target of known thickness (Table I). These methods usually agreed to within $\pm$ 20%, and thus the uncertainty in cross sections was often dominated by counting statistics. As previously noted, there also is a $\pm 3°$ angular spread in the secondary beam.

In order to verify the reaction mechanism and check the absolute cross section for $^{12}$C($^8$Li,$^7$Li)$^{13}$C$_{g.s.}$, we have measured [11] the inverse reaction $^{13}$C($^7$Li,$^8$Li)$^{12}$C$_{g.s.}$ at the appropriate $^7$Li bombarding energy. The cross sections for the two measurements agree with those expected from detailed balance, if we assume that only the g.s. $\rightarrow$ g.s. transitions are involved. This supports our assumption that $^{12}$C($^8$Li,$^7$Li$_{g.s.}$), rather than

TABLE III. ($^8$Li,$^7$Li) spectroscopic factors.

| Reaction | $E_x$ (MeV) | $J_i^\pi$ $0^+$ | $J_f^\pi$ | $S_{\text{expt}}$[a] | $S_{CK}$[b] |
|---|---|---|---|---|---|
| $^2$H $\rightarrow$ $^3$H | 0 | $0^+$ | $\frac{1}{2}^+$ | 1.0 | |
| $^9$Be $\rightarrow$ $^{10}$Be$_{g.s.}$ | 0 | $\frac{3}{2}^-$ | $0^+$ | 4.0 | 2.35 |
| $^9$Be $\rightarrow$ $^{10}$Be* | 3.37 | $\frac{3}{2}^-$ | $2^+$ | 0.2[c] | 0.21[d] |
| $^{12}$C $\rightarrow$ $^{13}$C$_{g.s.}$ | 0 | $0^+$ | $\frac{1}{2}^-$ | 0.8 | 0.61 |
| $^{12}$C $\rightarrow$ $^{13}$C* | 3.85 | $0^+$ | $\frac{5}{2}^+$ | 1.1 | 1.0 |
| $^{13}$C $\rightarrow$ $^{14}$C$_{g.s.}$ | 0 | $\frac{1}{2}^-$ | $0^+$ | 1.2 | 1.38 |
| $^{14}$N $\rightarrow$ $^{15}$N$_{g.s.}$ | 0 | $1^+$ | $\frac{1}{2}^-$ | 1.9 | 1.43 |
| $^{27}$Al $\rightarrow$ $^{28}$Al$_{g.s.}$ | 0 | $\frac{5}{2}^+$ | $3^+$ | $< 3$[e] | 0.6[f] |
| $^{58}$Ni $\rightarrow$ $^{59}$Ni | 5.4 | $0^+$ | $\frac{5}{2}^+$ | 0.2 | 0.15[g] |

[a]Deduced from normalization to FRDWBA calculations assuming ($^8$Li,$^7$Li$_{g.s.}$) is the dominant transfer mode. We assume $^8$Li$_{g.s.} \rightarrow ^7$Li$_{g.s.} + n$ has $S = 1.0$ (see text and Ref. [15]).

[b]Theoretical values [29] except as noted.

[c]Assumes $p_{\frac{1}{2}}$ neutron transfer.

[d]Assumes $p_{\frac{1}{2}}$ neutron transfer.

[e]Upper limit.

[f]T.P.G. Carola and J.G. Van der Baan, Nucl. Phys. **A173**, 414 (1971).

[g]M.S. Chowdury and H.M. Sen Gupta, Nucl. Phys. **A205**, 454 (1973).

$^{12}C(^{8}Li,^{7}Li_{0.47})$, is the dominant neutron-transfer mechanism, as the latter would not necessarily agree with the inverse $^{13}C(^{7}Li_{g.s.},^{8}Li)$ cross sections measured.

A feature of the $^{12}C(^{8}Li,^{7}Li)^{13}C$ spectrum (Fig. 6) is the unusually large cross section observed for the transition to the high-spin level ($J^{\pi} = 5/2^{+}$) in $^{13}C$ at $E_x \doteq 3.5$ MeV. This level is also seen [19] with large cross sections in $^{12}C(^{7}Li,^{6}Li)^{13}C$. The large cross sections are presumably the result of statistical spin factors, as well as the mostly pure $1d_{5/2}$ single-particle nature of this level (see below). However, as we will show, the highly favorable reaction $Q$ value for certain $^{8}Li$-induced reactions further enhances the neutron-transfer probability.

Angular distributions for most of the $(^{8}Li,^{7}Li)$ reactions studied are shown in Figs. 9 and 10. (Data on certain targets which consist only of measurements at a few forward angles are not shown.) The agreement between the latest measurements and those reported previously [5] is generally good, although the present data have much better statistics and cover a larger angular range, viz., $\theta_{lab} \rightarrow 45°$. Also, better $^{8}Li$ beam normalization procedures that should be more reliable have been used, based on Rutherford scattering.

Our measurements include limited data [5,11] for the reactions of $^{2}H(^{8}Li,^{7}Li)^{3}H$ and $^{2}H(^{8}Li,^{9}Be)n$. As previously noted, $^{8}Li$ reactions are part of a crucial chain of reactions which determine the abundance of $^{7}Li$ and heavier nuclei and therefore are of considerable interest in nuclear astrophysics. The present experiments indicate a rather significant rate for this channel, which again has $Q > 0$. In a separate set of measurements [27] dedicated to obtaining data specifically needed for nucleosynthesis calculations, cross sections for these channels were measured at $E(^{8}Li)$=6 to 14 MeV, corresponding to $E_{c.m.} \doteq 0.6$ to 2.5 MeV. These results will be reported elsewhere [27].

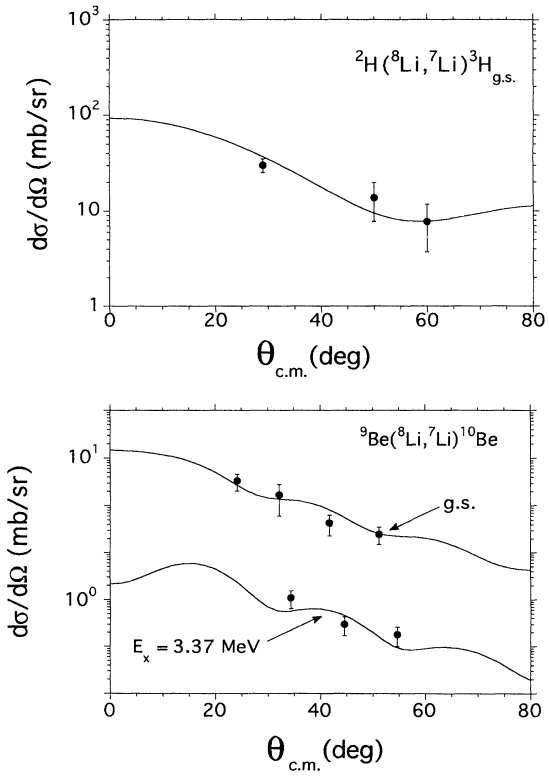


FIG. 9. Experimental and calculated $(^{8}Li,^{7}Li)$ cross sections, $E(^{8}Li) \doteq 14$ MeV.

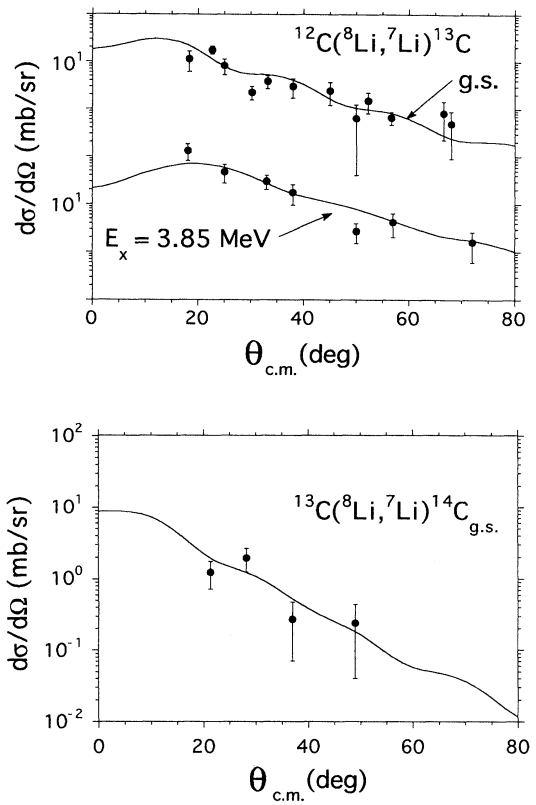


FIG. 10. Experimental and calculated $(^{8}Li,^{7}Li)$ cross sections, $E(^{8}Li) \doteq 14$ MeV.

### B. Spectroscopic factors

We have done finite-range distorted-wave Born-approximation (FRDWBA) calculations [24] for $(^{8}Li,^{7}Li)$ assuming a simple one-step *direct* neutron-transfer reaction. The required $^{8}Li$ and $^{7}Li$ OM parameters were obtained by suitably scaling our OM potential parameters deduced from $^{8}Li$ elastic scattering (Sec. III). As noted, the $^{8}Li$ OM potentials are similar to those observed for $^{7}Li$ and $^{6}Li$ and adequately fit elastic scattering data for the latter. The finite-range distorted-wave Born-approximation (FRDWBA) calculations shown in Figs. 9 and 10 are seen to adequately reproduce the overall shapes of the angular distribution data. However, since

multiple $\ell$ transfers are involved, one does not observe nor expect highly structured angular distributions.

The corresponding spectroscopic factors deduced from the FRDWBA calculations are given in Table III. They approximately follow experimental values obtained from stable-beam neutron transfers or from calculated shell-model values where available [26]. Hence, we believe the ($^8$Li,$^7$Li) reaction at $E(^8\text{Li}) \doteq 14$ MeV is primarily a *direct* single nucleon transfer reaction, as opposed to a compound-nucleus (CN) reaction or other nondirect process. Such CN reactions are often assumed to dominate at low bombarding energies, but this clearly may not be the case for certain RNB reaction channels, especially when $Q \gg 0$.

Of particular interest are the large observed neutron stripping cross sections to high-spin levels near $Q = Q_{\text{opt}} \approx 0$, such as the $^{12}\text{C}(^8\text{Li},^7\text{Li})^{13}\text{C}_{1d_{5/2}}$ ($E_x \doteq 3.5$ MeV) data which we noted. Such "quasielastic" processes, which may be a common feature of many RNB-induced reactions, can be highly favored by both the usual $(2J_f+1)$ spin statistics for nucleon stripping, as well as the optimal RNB $Q$ values (below). As discussed elsewhere [25], the FRDWBA calculations (Table III) for the near-barrier $^{58}\text{Ni}(^8\text{Li},^7\text{Li})^{59}\text{Ni}$ reaction also support the hypothesis of a direct neutron "tunneling" mechanism [31–33]. Thus, RNB-induced sub-barrier neutron tunneling [28,29] in heavy nuclei can also be large. This could provide a useful new tool for the study of single-particle levels in these nuclei, particularly for $A \geq 200$ where the location of many high-spin single-particle levels is still uncertain.

### C. $Q$ windows and enhanced cross sections

As seen above, reactions induced by RNB and stable nuclei can differ greatly in their reaction $Q$ values. This can be illustrated by isolating the $Q$-value dependence [28–30] of typical reactions. As an example, if one does a direct neutron-transfer calculation (FRDWBA) as a function of $E$(Li), i.e., an excitation function for $^8$Li($^2$H,$^3$H), where $Q \doteq +4$ MeV, and $^7$Li($^2$H,$^3$H), where $Q \doteq -1$ MeV, rather large $Q$-value related effects are observed [6,11]. In Fig. 11, we show the calculated excitation functions where we have normalized the $^2$H($^8$Li,$^7$Li)$^3$He cross section to our experimental data. (In order to isolate only the $Q$-value effects, the OM parameters and transfer form factors are kept identical for these calculations.) The shapes and magnitudes of the calculated cross sections as a function of $E$(Li) are, as expected, very different. Particularly, as $E$(Li)$\rightarrow$0, i.e., as $E_{\text{c.m.}}$ approaches the region of astrophysical energies (a few hundred keV), the differences become quite significant (Fig. 11). This illustrates the high enhancement RNB-induced direct-reaction cross sections, with $Q > 0$, can exhibit even at relatively low $E_{\text{c.m.}}$. There may also be enhancements due to the nuclear alignment of a low-energy RNB analogous to that calculated [31] for deuteron projectiles (Oppenheimer-Phillips effect). Assumptions made about the absolute rates and energy dependence of RNB-induced reactions of astrophysical importance must take these features into consideration.

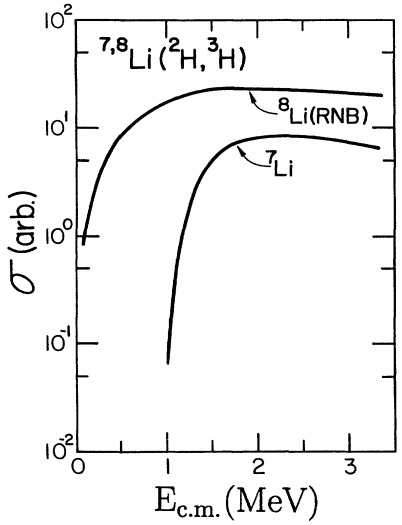


FIG. 11. Calculated (FRDWBA) direct neutron-transfer integrated cross sections for the RNB $^8$Li($^2$H,$^3$H) and stable-beam $^7$Li($^2$H,$^3$H) reactions in the same (but arbitrary) units.

Likewise, $Q$-value effects ($Q$ windows) are also significant for other, heavier target nuclei. This is illustrated in Fig. 12 where we display a typical $Q$-value dependence calculated for the $^{12}\text{C}(^8\text{Li},^7\text{Li})$ and $^{12}\text{C}(^7\text{Li},^6\text{Li})$ reactions. One notes the "$Q$ window" in the cross section and the corresponding enhanced cross section for $^8$Li-induced reactions to the $^{13}\text{C}_{\text{g.s.}}$ and excited states. This confirms our observation for $^{12}\text{C}(^8\text{Li},^7\text{Li})^{13}\text{C}_{5/2+}$ ($E_x \doteq 3.5$ MeV), of large cross sections where $Q \approx Q_{\text{opt}}$. Again, as $E$(Li)$\rightarrow$0 direct transfers can remain important in RNB-induced reactions even on heavier nuclei.

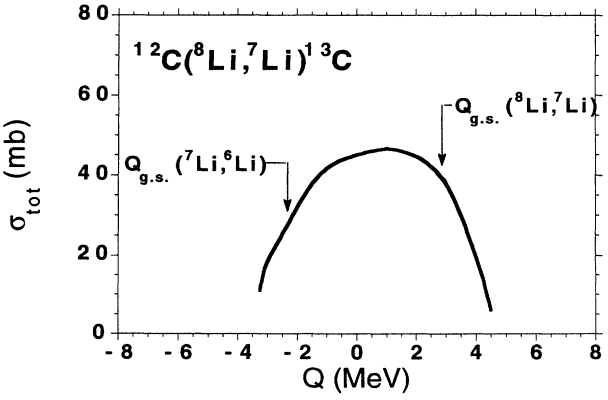


FIG. 12. Calculated $Q$-value dependence of the $^{12}\text{C}(^7\text{Li},^6\text{Li})$ and $^{12}\text{C}(^8\text{Li},^7\text{Li})$ cross sections, $E(^8\text{Li}) \doteq 14$ MeV, with the appropriate $^{12}\text{C} \rightarrow ^{13}\text{C}_{\text{g.s.}}$ $Q$ values indicated.

## V. THE ($^8$Li,$\alpha$) REACTION

### A. Data

As noted in the $\Delta E$-$E$ spectra shown in Figs. 1–3, very-high-energy $\alpha$ particles are apparently observed from highly exothermic ($^8$Li,$\alpha$) reactions (Table I). Although the secondary $^8$Li beam (Sec. II) has a small (few %) fraction of $^4$He$^{1+,2+}$ (as well as $^6$He$^{1+,2+}$, etc.) the observed $\alpha$-particle energy spectra extend well beyond the known location of the $^4$He (and $^6$He) contamination.

Large cross sections were observed for the $^1$H($^8$Li, $\alpha$)$^5$He$_{g.s.}$ reaction from the $^{nat}CH_2$ and melamine targets and are presented elsewhere [32]. The $\alpha$-particle energy spectra and cross sections observed for $^9$Be and $^{12}$C other targets (Figs. 13 and 14) are consistent with those expected for an evaporation spectrum from ($^8$Li, $\alpha$) and appear to be similar to ($^{6,7}$Li, $\alpha$) data observed at similar bombarding energies [33]. However, unlike $^6$Li and $^7$Li, the primary breakup modes of $^8$Li are via neutron emission (viz., $^8\text{Li} \rightarrow {}^7\text{Li}$) rather than $\alpha$-particle emission (viz., $^7\text{Li} \rightarrow \alpha + t$ and $^6\text{Li} \rightarrow \alpha + d$), so we do not expect very-high-energy $\alpha$ particles directly from $^8$Li breakup. Instead, such $\alpha$ particles would require the sequential breakup $^8\text{Li} \rightarrow {}^7\text{Li}^* + n \rightarrow \alpha + t + n$ and would thus appear at low $E_\alpha$ ($\ll E_{\text{beam}}$). Also, due to the three-body kinematics, these alphas would not be particularly forward peaked in $\theta_{\text{lab}}$.

In the case of $^{12}$C($^8$Li,$\alpha$)$^{16}$N, we observe (Fig. 14) a strong emission of $\alpha$ particles to a group of levels near the $^{16}N_{g.s.}$. This feature can be explained, at least qualitatively, by the $Q$ value and spin statistics when one assumes a CN reaction mechanism (see below). However, unlike ($^6$Li, $\alpha$) and ($^7$Li, $\alpha$), which also show enhanced cross sections to selective levels [36], we cannot attribute ($^8$Li, $\alpha$) cross sections to contributions from a direct cluster-transfer mechanism as this would require transfer of a $^4$H "cluster." This seems unlikely since, as noted, $^8$Li has the dominant spectroscopic structure: $^7\text{Li}+n = (\alpha + t) + n$, where the triton and neutron are not particularly spatially correlated.

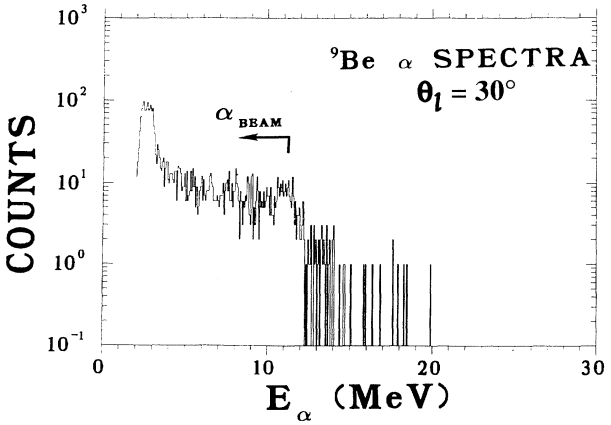


FIG. 13. Experimental alpha-particle energy spectra of $^9$Be($^8$Li, $\alpha$), $E(^8\text{Li}) \doteq 14$ MeV. The $\alpha$-particle beam contamination is indicated.

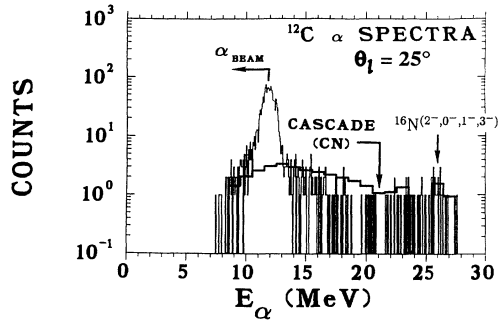


FIG. 14. Experimental alpha-particle energy spectra of $^{12}$C($^8$Li, $\alpha$), $E(^8\text{Li}) \doteq 14$ MeV, compared with a CASCADE (CN) calculation. The $\alpha$-particle beam contamination is indicated.

A limited amount of ($^{6,7}$Li, $\alpha$) data have been published [33] for $^{6,7}$Li + $^{12}$C at $E(^7\text{Li}) = 14 - 20$ MeV. We can therefore compare (Li, $\alpha$) spectra and reaction data for $^{6,7}$Li to those from $^8$Li. While one again observes significant ($^6$Li, $\alpha$) and ($^7$Li, $\alpha$) production spectra (Fig. 15), many, if not most, of the forward-angle $\alpha$ particles appear to arise from $^7\text{Li} \rightarrow \alpha + t$, $^6\text{Li} \rightarrow \alpha + d$ or related transfer mechanism, as the spectral shape (and angular

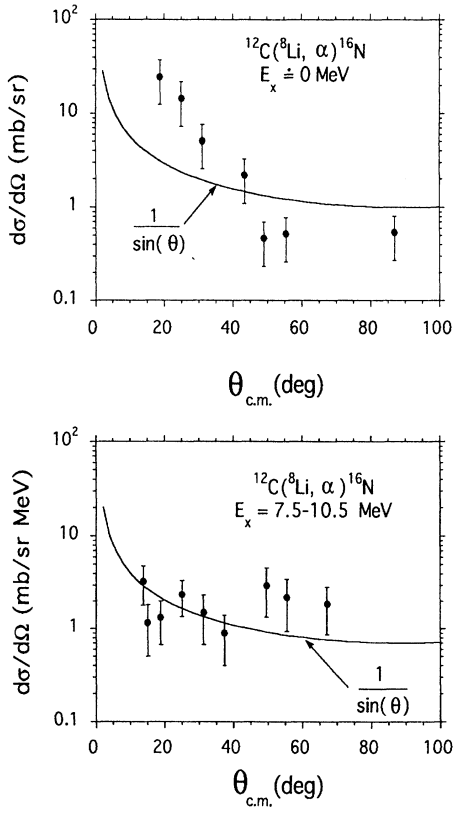


FIG. 15. Experimental angular distribution for the reaction $^{12}$C($^8$Li, $\alpha$), $E(^8\text{Li}) \doteq 14$ MeV, compared with a $1/\sin(\theta_{\text{c.m.}})$ distribution expected for a CN reaction.

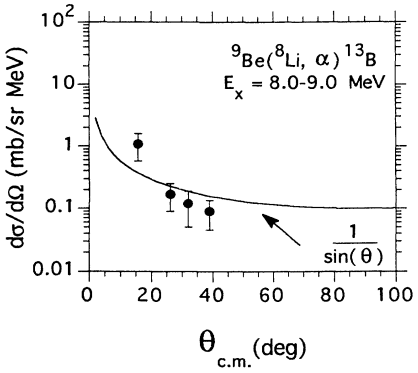


FIG. 16. Experimental angular distribution for the reaction $^9$Be($^8$Li, $\alpha$), $E(^8\text{Li}) \doteq 14$ MeV, compared with a $1/\sin(\theta_{\text{c.m.}})$ distribution expected for a CN reaction.

distributions) differ from those observed here for ($^8$Li, $\alpha$) and other CN reactions.

Angular distributions for high-energy $\alpha$-particle events observed in $^{12}$C($^8$Li, $\alpha$) and $^9$Be($^8$Li, $\alpha$), summed over various regions of excitation energy, indicate an approximate $1/\sin\theta$ dependence (Figs. 15 and 16). This is again indicative of a compound-nucleus (CN) fusion evaporation mechanism [34]. As observed [33] in ($^6$Li, $\alpha$) and ($^7$Li, $\alpha$) we also observe somewhat forward-peaked angular distributions for the most energetic alpha particles. This feature in ($^6$Li, $\alpha$) and ($^7$Li, $\alpha$) data is attributed to direct transfer of a deuteron or triton, respectively, but again direct $^4$H transfer does not seem plausible to explain this feature in the ($^8$Li, $\alpha$) data.

The typical spectral slope parameters $[N_\alpha(E_\alpha) \equiv N_0^{-E_\alpha/T_\alpha}]$ correspond to $T_\alpha \approx 3$ MeV, which is a typical CN temperature [34]. The $^{12}$C($^8$Li, $\alpha$)$^{16}$N* cross sections are typically a few mb/sr MeV at $E_x \approx 7.5$ to 10 MeV, with an estimated total integrated $^{12}$C($^8$Li, $\alpha$) cross section of 14 mb/MeV at these energies assuming a $1/\sin\theta$ dependence that persists to 180°.

### B. Analysis using compound nucleus code (CASCADE)

Compound-nucleus (CN) calculations [34] of $^8$Li+$^{12}$C$\rightarrow^{20}$F*$\rightarrow^{16}$N* + $\alpha$, using the statistical CN program CASCADE [35] with the appropriate, discrete levels known in $^{16}$N and $^{20}$F (but neglecting isospin), predict cross sections of about 24 mb/sr MeV at $E_x \doteq 8$ MeV in the CN $^{16}$N*. Still, these predictions are considerably larger (×2 to ×4) than our ($^8$Li, $\alpha$) measurements indicate. A similar discrepancy has been reported for $^8$Li($p, n$) data obtained in related experiments [36]. This discrepancy implies that either (i) our optical-model parameters overpredict the $^8$Li total inelastic reaction cross sections or (ii) less than half of the calculated OM total inelastic reaction cross sections ($\sigma_R$) appears in CN channels. Since our calculated $^8$Li + $^{27}$Al total inelastic reaction cross section (Table II) is in excellent agreement with the direct measurements of $\sigma_R$ for $^6$Li + $^{28}$Si of 1490±80 [$E(^6\text{Li}) = 18$ to 28 MeV] by Warner *et al.* [37], the latter (ii) may be the likely explanation. This would be consistent with the large direct transfer cross sections observed, the broad $Q$ windows hence excitation region for $^8$Li-induced direct reactions, and the possibility of significant $^8$Li breakup channels.

As in the case of the ($^8$Li,$^7$Li) reaction, the large positive $Q$ value for ($^8$Li, $\alpha$) and other specific RNB CN reactions suggests that many of these could have significant cross sections even as $E(\text{RNB}) \rightarrow 0$, i.e., at collisional energies relevant to nucleosynthesis.

Although high-energy protons, deuterons, and tritons are also presented in some of our spectra, the ΔE detectors used were too thin to obtain any quantitative information for ($^8$Li,$p$), ($^8$Li,$d$), or ($^8$Li,$t$). The CASCADE predictions for these CN channels are shown in Fig. 17 and compared with a similar calculation done for $^7$Li + $^{12}$C. The CASCADE CN calculations suggest that the ($^8$Li,2$n$) and ($^8$Li,2$n\alpha$) channels [as well as the ($^8$Li,$n\alpha$) channels] should be enhanced relative to similar $^{6,7}$Li CN reactions, as one might expect for a neutron-rich RNB. In general, high-multiplicity channels are favored since several CN decays may be required to reach particle stability with an RNB projectile. If even more neutron-rich projectiles such as $^{6,8}$He, $^{9,11}$Li, etc. are employed, the corresponding channels would likely be even further enhanced.

## VI. CONCLUSIONS

The elastic scattering of $^8$Li from various nuclei at $E(^8\text{Li}) = 13$ to 20 MeV can be well represented by a conventional optical-model potential which, in addition, also provides adequate fits to low-energy $^{6,7}$Li data. No unusual increase in the strong absorption radius for $^8$Li is needed. A large inelastic excitation probability and $B[E2\uparrow]$ for $^8\text{Li}^*_{0.98}$ is observed, as are large cross sections for the ($^8$Li,$^7$Li) reaction, particularly near the "quasielastic" $Q$ values. The ($^8$Li,$^7$Li) reaction appears to proceed by direct single-neutron transfer of the loosely bound valence neutron of $^8$Li, and thus should persist even at low $^8$Li bombarding energies due to its exother-

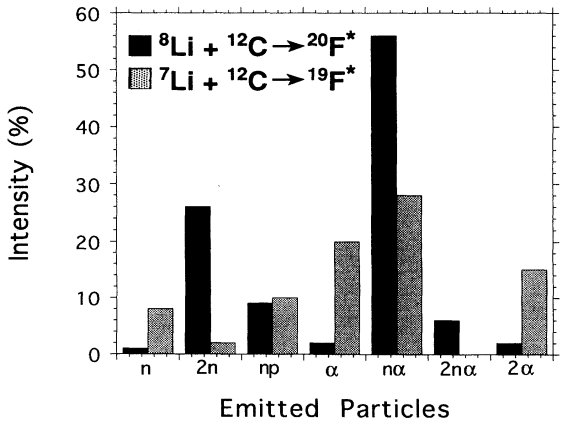


FIG. 17. CASCADE CN calculations for $^8$Li + $^{12}$C compared with those for $^7$Li + $^{12}$C for $E(^8\text{Li}) \doteq 14$ MeV.

mic nature. Yet another important reaction channel appears to be ($^8$Li, $\alpha$) which has the characteristics of a fusion-evaporation CN reaction, although again with a very positive $Q$ value and hence a corresponding production of very energetic $\alpha$ particles even as $E(\mathrm{Li}) \rightarrow 0$. All of these channels should be considered in nucleosynthesis and other calculations involving $^8$Li and other neutron-rich RNB.

## ACKNOWLEDGMENTS

This work was supported by NSF Grants PHY-8605907, PHY-8911831, PHY-8803035, PHY-8900070, PHY-9100078, PHY-9122067, and PHY-9208468. The authors thank Sunil Dixit, David Hotz, Ed Berners, Robert Kryger, and Richard Tighe for their assistance during various stages of these experiments.

[1] C.E. Rolfs and W.S. Rodney, *Cauldrons in the Cosmos* (University of Chicago Press, Chicago, 1988).
[2] J.H. Applegate, C.J. Hogan, and R.J. Scherrer, Astrophys. J. **329,** 592 (1988).
[3] R.A. Malaney and W.A. Fowler, Astrophys. J. **333,** 14 (1988).
[4] T. Kajino and R.N. Boyd, Astrophys. J. **359,** 267 (1990).
[5] F.D. Becchetti, W.Z. Liu, D.A. Roberts, J.W. Jänecke, J.J. Kolata, A. Morsad, X.J. Kong, and R.E. Warner, Phys. Rev. C **40**, R1104 (1989).
[6] W.Z. Liu, F.D. Becchetti, J. Brown, J.W. Jänecke, D.A. Roberts, J.J. Kolata, A. Morsad, R. Smith, X.J. Kong, and R.E. Warner, in *Proceedings of the First International Conference on Radioactive Nuclear Beams,* edited by W.D. Myers, J.M. Nitschke, and E.B. Norman (World Scientific, Singapore, 1990), p. 499.
[7] I. Tanihata *et al.,* Phys. Lett. **160B,** 380 (1985).
[8] Y. Suzuki, K. Ikeda, and H. Sato, Prog. Theor. Phys. Lett. **83,** 180 (1990).
[9] G.R. Bertsch and J. Foxwell, Phys. Rev. C **41,** 1300 (1990).
[10] F.D. Becchetti, W.Z. Liu, D.A. Roberts, J.W. Jänecke, J.J. Kolata, A. Morsad, X.J. Kong, and R.E. Warner, in *Proceedings of the International Symposium on Heavy Ion Physics and Nuclear Astrophysical Problems,* edited by S. Kubono, M. Ishihara, and T. Nomura (World Scientific, Singapore, 1989), p. 277; F.D. Becchetti *et al.,* Nucl. Instrum. Methods **B56/57,** 54 (1991).
[11] W.Z. Liu, Ph.D. thesis, University of Michigan, 1990 (unpublished).
[12] J.J. Kolata, A. Morsad, X.J. Kong, R.E. Warner, F.D. Becchetti, W.Z. Liu, D.A. Roberts, and J.W. Jänecke, Nucl. Instrum. Methods **B40/41,** 503 (1989).
[13] F.D. Becchetti, J. Brown, J.W. Jänecke, W.Z. Liu, D.A. Roberts, J.J. Kolata, R. Smith, K.L. Lamkin, A. Morsad, and R.E. Warner, in *Proceedings of the First International Conference on Radioactive Nuclear Beams* [6], p. 305.
[14] J.J. Kolata, R. Smith, K.L. Lamkin, A. Morsad, F.D. Becchetti, J. Brown, J.W. Jänecke, W.Z. Liu, and D.A. Roberts, in [6], p. 201.
[15] J. Brown, F.E. Becchetti, W.Z. Liu, J.W. Jänecke, D.A. Roberts, J.J. Kolata, A. Morsad, and R.E. Warner, in [6], p. 372.
[16] R.J. Smith, J.J. Kolata, K.L. Lamkin, A. Morsad, K. Ashktorab, F.D. Becchetti, J. Brown, J.W. Jänecke, W.Z. Liu, and D.A. Roberts, Phys. Rev. C **43,** 761 (1991).
[17] J.A. Brown, F.D. Becchetti, J.W. Jänecke, K. Ashktorab, D.A. Roberts, J.J. Kolata, R.J. Smith, K.L. Lamkin, and R.E. Warner, Phys. Rev. Lett. **66,** 2452 (1991).
[18] M.F. Vineyard, J. Cook, K.W. Kemper, and M.N. Stephens, Phys. Rev. C **30,** 916 (1984).
[19] P. Schumacher, N. Veta, H.H. Duhm, K.I. Kubo, and W.J. Klages, Nucl. Phys. **A212,** 573 (1973).
[20] L.T. Chua, F.D. Becchetti, J. Jänecke, and F.L. Milder, Nucl. Phys. **A273,** 243 (1976).
[21] A. Nadasen, M. McMaster, G. Gunderson, A. Judd, S. Villanueva, P. Schwandt, J.S. Winfield, J. van der Plicht, R.E. Warner, F.D. Becchetti, and J.W. Jänecke, Phys. Rev. C **37,** 132 (1988).
[22] J.R. Comfort, Program CUPID, Comput. Phys. Commun. **16,** 35 (1978).
[23] D. Fick, G. Grawert, and I. Turkiewicz, Phys. Rep. **214,** 1 (1992).
[24] P.D. Kunz, Program DWUCK5, modified by J.D. Comfort (unpublished).
[25] F.D. Becchetti *et al.,* Proceedings of the Third International Conference on Radioactive Beams, edited by D. Morrissey *et al.* (unpublished).
[26] S. Cohen and D. Kurath, Nucl. Phys. **A101**, 1 (1967); B.A. Brown (private communication).
[27] M.M. Farrell, R.N. Boyd, J.D. Kalen, X. Gu, J.J. Kolata, R.J. Smith, K.L. Lamkin, R. Tighe, K. Ashktorab, and F.D. Becchetti, in *Proceedings of the International Workshop on Unstable Nuclei in Astrophysics,* edited by S. Kubono and T. Kajino (World Scientific, Singapore, 1992), p. 332.
[28] P.J.A. Buttle and L.J.B. Goldfarb, Nucl. Phys. **A176,** 299 (1971).
[29] A.R. Barnett, W.R. Phillips, P.J.A. Buttle, and L.J.B. Goldfarb, Nucl. Phys. **A176,** 321 (1971).
[30] P.R. Christensen, V.I. Manko, and R.J. Nickles, Nucl. Phys. **A207,** 33 (1973).
[31] J.R. Oppenheimer and M. Phillips, Phys. Rev. **48,** 500 (1935).
[32] F.D. Becchetti, J.A. Brown, W.Z. Liu, J.W. Jänecke, D.A. Roberts, J.J. Kolata, R.J. Smith, K. Lamkin, A. Morsad, R.E. Warner, R.N. Boyd, and J.D. Kalen, Nucl. Phys. **A550,** 507 (1992).
[33] I. Tserruya, B. Rosner, and K. Bethge, Nucl. Phys. **A213,** 22 (1973); K. Meier-Ewert, K. Bethge, and K.O. Pfeiffer, *ibid.* **A110,** 142 (1968).
[34] R. Stokstad, in *Treatise on Heavy-ion Science, Vol. 3,* edited by D. Allan Bromley (Plenum, New York, 1985).
[35] F. Pühlhofer, Nucl. Phys. **A280,** 267 (1977).
[36] D.D. Caussyn, N.R. Fletcher, K.W. Kemper, E.E. Towers, J.J. Kolata, K. Lamkin, R.J. Smith, F.D. Becchetti, J.A. Brown, J.W. Jänecke, D.A. Roberts, and D.L. Gay, Phys. Rev. C **47**, 387 (1993).
[37] R.E. Warner *et al.,* Nucl. Instrum. Methods **A314,** 113 (1992).